SIMULATING THE EFFECT OF WIND-DRIVEN SHEAR STRESS ON TURBULENT OPEN-CHANNEL FLOW

SHOKO SUGIMOTO
Kyushu University, Kasuga, Fukuoka, Japan, sugimoto@esst.kyushu-u.ac.jp

KO SHIRAKAWA
Kyushu University, Kasuga, Fukuoka, Japan, shirakawa@esst.kyushu-u.ac.jp

YUJI SUGIHARA
Kyushu University, Kasuga, Fukuoka, Japan, sugihara.yuji.290@m.kyushu-u.ac.jp

MICHIO SANJOU
Kyoto University, Katsura, Kyoto, Japan, michio.sanjou@water.kuciv.kyoto-u.ac.jp

TAKAAKI OKAMOTO
Kyoto University, Katsura, Kyoto, Japan, okamoto.takaaki.8x@kyoto-u.ac.jp

ABSTRACT

In order to investigate characteristics of open-channel flow under wind-driven shear stress on the water surface, we carry out numerical simulations by using the direct numerical simulation, i.e., DNS, and RANS with the standard k- ε model. The vertical distributions of the streamwise velocity and the Reynolds stress vary depending on the sign and magnitude of the surface shear stress. The numerical results from DNS demonstrate that under the condition of negative shear stress, the streamwise velocity around the half-water depth is increased than that in the case of no shear stress. The surface divergence calculated from DNS is confirmed to be universally scaled with the Taylor microscale regardless of the positive or negative sign of the shear stress. Though the volume flow rate doesn't change regardless of the variation of the surface shear stress, the scalar flux at the water surface is found to be decreased in the case of negative shear stress. This suggests that the direction of wind-driven shear stress relative to the main flow becomes important for the scalar transport. In addition, the cross-correlation coefficients between the scalar flux and physical quantities such as the surface divergence and the vorticities close to the water surface are investigated to identify turbulent vortex structure controlling the air-water scalar transport. It has been concluded that the scalar flux increases considerably when the vortex structure is arranged so as to induce a strong upward flow toward the water surface.

Keywords: *Open-channel flow, wind stress, turbulence, scalar transport, DNS*

1. INTRODUCTION

Several studies on characteristics of turbulent fields affected by wind-driven shear stress on the water surface have been made primarily for wind-wave turbulence without background flow (e.g., Matsunaga and Uzaki (2002)). However, a relatively strong wind blows frequently above the surface of river, having the mean flow. Open channel flow, which can be recognized as a physical model of river flow turbulence, is most basic and highly applicable in the field of hydraulic engineering, and much research has been accumulated on its turbulent field (see Tominaga (2010)). Therefore, it is of interest to investigate how the turbulent structure of open-channel flow varies when wind-driven shear stress acts on the water surface.

The response of turbulent fields to wind stress has been mainly studied experimentally until now. Nezu et al. (2004) investigated the relationship between turbulence and water surface fluctuation in the case where wind stress acts on the water surface in open channel flow. They tried to classify the experimental data based on the ratio of the air side shear stress on the water surface to the bottom shear stress. Such an indicator is considered to be important in defining and interpreting the physical phenomena in this problem. Furthermore, Sanjou and Nezu (2011) examined the change of turbulent flow according to the wave development by blowing air above the water surface in a laboratory wind-water tunnel tank. Though several experimental approaches have been attempted so far, but there are no clear findings or conclusions about the response of open channel turbulence to wind-driven shear stress. This problem may be also redefined as an examination of the effect of wind stress on mass transport in river flow.

In this study, we investigate the effect of the surface shear stress on open-channel flow turbulence through numerical simulations. In particular, we aim at clear findings about the characteristics of the turbulent flow

affected by the surface shear stress; thus we simplify the analytical object as much as possible. The numerical models used in this study are the direct numerical simulation (DNS) and the RANS simulation with the standard k-ε model, which is one of the simplest RANS models. Furthermore, we confirm how a scaling relation for the divergence of horizontal velocities on the water surface, i.e., the surface divergence, proposed in previous studies (see Tsumori and Sugihara (2007) and Sanjou et al. (2015)), depends on the surface shear stress, and investigate the dependence of scalar transport at the water surface on the surface shear stress. Finally, we discuss the cross-correlation coefficients between the surface scalar flux and the turbulence characteristics close to the water surface to identify turbulent motions controlling the air-water scalar transport.

2. OUTLINE OF NUMERICAL SIMULATIONS

Let us consider the case where shear stress acts on the water surface $\rho u_{\tau s}^2$ (hereinafter referred to as surface shear stress) in an open channel with the bottom slope $\sin\theta$ and water depth h. Here, ρ is the density of water and $u_{\tau s}$ is the water side friction velocity, corresponding to the surface shear stress. For such a uniform flow, the gravitational and the surface shear forces are balanced with the bottom shear force, so that the following relationship holds

$$\frac{\rho g h \sin\theta}{\rho u_{\tau b}^2} = 1 - \tau_s^* , \tag{1}$$

where τ_s^* is defined as

$$\tau_s^* \equiv \frac{\rho u_{\tau s}^2}{\rho u_{\tau b}^2}. \tag{2}$$

Here, τ_s^* is the dimensionless surface shear stress, indicating the ratio of the surface shear stress to the bottom shear stress $\rho u_{\tau b}^2$. It should be noted that $\tau_s^* < 1$ holds in the case where there exists the background channel flow. Therefore, we can investigate the response characteristics of open-channel turbulence to the surface shear stress by systematically changing the value of τ_s^*. In this study, we set $\tau_s^* = 0.0,\ \pm 0.1,\ \pm 0.2,\ \pm 0.3$, for which only the shear stress parallel to the direction of main flow acts on the water surface.

2.1 Direct numerical simulation (DNS)

For performing DNS, the space coordinates x_i, time t, flow velocities u_i, and pressure p are non-dimensionalized by using $u_{\tau b}$ and water depth h. The basic equations consist of the continuity equation for incompressible fluid, the Navier-Stokes equation and the advection-diffusion equation for a passive scalar as follows:

$$\left.\begin{aligned} &\frac{\partial u_i^*}{\partial x_i^*} = 0 \\ &\frac{\partial u_i^*}{\partial t^*} + u_j^* \frac{\partial u_i^*}{\partial x_j^*} = -\frac{\partial p^*}{\partial x_i^*} + \frac{1}{Re_\tau}\left(\frac{\partial^2 u_i^*}{\partial x_j^* x_j^*}\right) + \frac{\delta_{1i}}{Fr_\tau^2} \\ &\frac{\partial c^*}{\partial t^*} + u_j^* \frac{\partial c^*}{\partial x_j^*} = \frac{1}{ScRe_\tau}\frac{\partial^2 c^*}{\partial x_j^* \partial x_j^*} \ , \end{aligned}\right\} \tag{3}$$

where the subscript $*$ denotes the dimensionless quantity, and parameters Fr_τ, Re_τ and Sc are defined as

$$\frac{1}{Fr_\tau^2} \equiv \frac{gh\sin\theta}{u_{\tau b}^2} = 1 - \tau_s^*, \quad Re_\tau \equiv \frac{u_{\tau b} h}{\nu}, \quad Sc \equiv \frac{\nu}{D}. \tag{4}$$

The parameters and boundary conditions in the numerical simulation using DNS are summarized in Table 1 (see Sugihara et al. (2011)). The boundary conditions for the flow velocities on the water surface are given by

$$\frac{1}{Re_\tau}\frac{\partial u_1^*}{\partial x_2^*} = \tau_s^*, \quad u_2^* = 0, \quad \frac{\partial u_3^*}{\partial x_2^*} = 0 . \tag{5}$$

Here, the coordinate system is a three-dimensional rectangular one, defining x_1^* as the streamwise direction, x_2^* the vertical direction taken upward from the bottom, and x_3^* the spanwise direction. In addition, the periodic boundary conditions are imposed on the side boundaries, and the no-slip condition is imposed on the bottom surface. The analysis is performed under the condition of no surface fluctuation in the vertical direction, so that the vertical displacement of the water surface is not considered and this assumption may influence the anisotropy of near-surface turbulence. Also, the surface shear stress is kept to be constant on the water surface in this study. Note that the averaged value of the shear stress on the bottom surface is given by $\rho u_{\tau b}^2$, but its local value varies spatiotemporally on the bottom surface. After the next sections, for convenience, each quantity is represented as follows:

$$\left.\begin{array}{l} x_1^* \equiv x^*,\ \ x_2^* \equiv y^*,\ \ x_3^* \equiv z^* \\ u_1^* \equiv u^*,\ \ u_2^* \equiv v^*,\ \ u_3^* \equiv w^* . \end{array}\right\} \tag{6}$$

Table 1. Calculation method and conditions for DNS

Numerical algorithm	Simplified MAC method	
Differential approximation	4^{th}-order central-differences, Lagrange's interpolation	
Time evolution	$(1^{st}\ step)$ Explicit Euler method $(2^{nd}\ step)$ 2^{nd}- order Adams-Bashforth method	
Size of comp. domain	Streamwise x^* : 7.68, Spanwise z^* : 3.84, Vertical y^* :1.0	
Number of comp. grids	$Re_\tau = 150$: (Nx, Ny, Nz) = (128, 129, 128)	
Grid spacing	$Re_\tau = 150$: $(\Delta x^*, \Delta y^*, \Delta z^*)$=(0.06,7.4 × 10^{-4}~1.5 × 10^{-2},0.03)	
Time difference, Total times	Δt^* =5.0× 10^{-5}, $t^* = 15$	
Non-dimensional Parameters	$Re_\tau = 150$, $S_c = 1.0$, $1/Fr_\tau^2$ = 1- τ_s^*, τ_s^* =-0.3,-0.2,-0.1,0,0.1,0.2,0.3	
Boundary conditions	x^*, z^* axis boundaries	y^* axis boundary
	u^*, v^*, w^*, p^*: Periodic	u^*, w^* at y^*=0: Dirichlet and at y^*=1: Neumann v^*: Dirichlet, p^*: Neumann

2.2 RANS simulation using the standard k-ε model

The outline of the simulation using the standard k-ε model (see Nakayama and Yokojima (1999)), which is the most representative RANS model, is described here, but we leave out their basic equations because of space limitations of paper. For the simulation with the k-ε model, the non-dimensional quantities are defined as

$$y \equiv h\eta,\ \ t \equiv \frac{h}{U_\delta}\tilde{t},\ \ U \equiv U_\delta \tilde{U},\ \ k \equiv k_\delta \tilde{k},\ \ \varepsilon \equiv \varepsilon_\delta \tilde{\varepsilon}\ , \tag{7}$$

where U is the averaged streamwise velocity, k the turbulent kinetic energy, ε the energy dissipation rate, and ˜ denotes the dimensionless quantity. U_δ, k_δ and δ are also defined as follows:

$$\left.\begin{array}{l} U_\delta \equiv u_{\tau b}\left[\dfrac{1}{\kappa} ln\left(Re_\tau\left(\dfrac{\delta}{h}\right)\right) + A_r\right] \\ k_\delta \equiv \dfrac{u_{\tau b}^2}{\sqrt{C_\mu}}, \varepsilon_\delta \equiv \dfrac{u_{\tau b}^3}{\kappa\delta}\ , \end{array}\right\} \tag{8}$$

where κ (= 0.41) is the Karman constant and A_r a constant to be 5.3 for the smooth surface. The closure model constants are given by $\sigma_k = 1.0$, $\sigma_\varepsilon = 1.3$, $C_1 = 1.44$, $C_2 = 1.92$ and $C_u = 0.09$. Also, δ/h is the wall boundary layer thickness depending on Re_τ, and we give 0.08 for $Re_\tau = 150$ on the basis of comparison with the DNS results. In this numerical experiment, the standard k-ε model is used, and only the upper layer above δ/h where the effect of the low Reynolds number effect due to the wall can be ignored is calculated. Since the low Reynolds number effect by the presence of the wall surface is ignored in the standard k-ε model, we simulate the turbulent structure in only upper layer from $\eta = \delta/h$. The eddy viscosity and the damping function of turbulence in the vicinity of the water surface f_s become

$$\left.\begin{array}{l} \tilde{\nu}_t = C_\mu f_S(\eta)\dfrac{\tilde{k}^2}{\tilde{\varepsilon}} \\ f_S(\eta) \equiv 1 - \exp\left(-A_s\dfrac{h\varepsilon_s}{k_s^{3/2}}(1-\eta)\right) \\ \qquad = 1 - \exp\left(-B_s(1-\eta)\right)\ , \end{array}\right\} \tag{9}$$

where k_s and ε_s included in the damping function represent the turbulent kinetic energy and the energy dissipation rate at the water surface, respectively. In this study, when $B_s > 18$ or $B_s < 18$, the variation of the vertical distribution of turbulence near the water surface became steeper or gentler than that of DNS. Therefore, we adopt $B_s = 18$ as a result of tuning, but the validity of this value should be examined in a future study. The grid width used for the numerical calculation is 0.005, and the boundary conditions are given as follows:

$$\left.\begin{array}{c} \tilde{U} = 1,\ \ \tilde{k} = 1,\ \ \tilde{\varepsilon} = 1\ \ \text{at}\ \ \eta = \dfrac{\delta}{h} \\ \left(\tilde{\nu}_t + \dfrac{1}{Re_\tau}\dfrac{C_\mu}{\kappa}\dfrac{h}{\delta}\right)\dfrac{\partial\tilde{U}}{\partial\eta} = \left(\dfrac{C_\mu}{\kappa}\dfrac{h}{\delta}\dfrac{u_{\tau b}}{U_\delta}\right)\tau_s^*,\ \ \dfrac{\partial\tilde{k}}{\partial\eta} = 0,\ \ \tilde{\varepsilon} = \dfrac{\left(\dfrac{\delta}{h}\right)}{\left(\dfrac{y'}{h}\right)}\tilde{k}^{\frac{3}{2}}\ \text{at}\ \eta = 1 \end{array}\right\} \tag{10}$$

with y'/h being a certain turbulence scale close to the water surface, for which we adopt a recommended value of 0.07 by Nakayama and Yokojima (1999). In this study, the condition for the surface shear stress in Eq. (10) is given by using the form of the central difference at a grid point below the one mesh from the water surface, and we set the streamwise velocity at the surface to satisfy these relationships.

3. RESULTS AND DISCUSSION

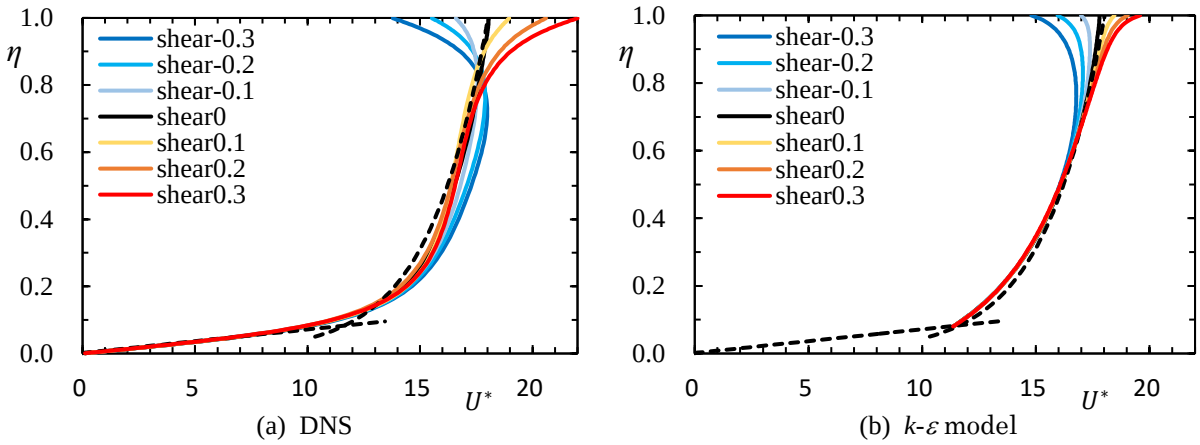

(a) DNS (b) k-ε model

Figure 1. Response of averaged streamwise velocity distributions to τ_s^* (DNS vs. k-ε model, $Re_\tau = 150$)

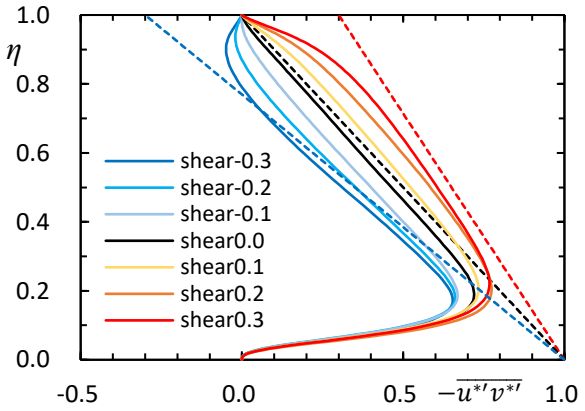

Figure 2. Reynolds stress distribution (DNS, $Re_\tau = 150$)

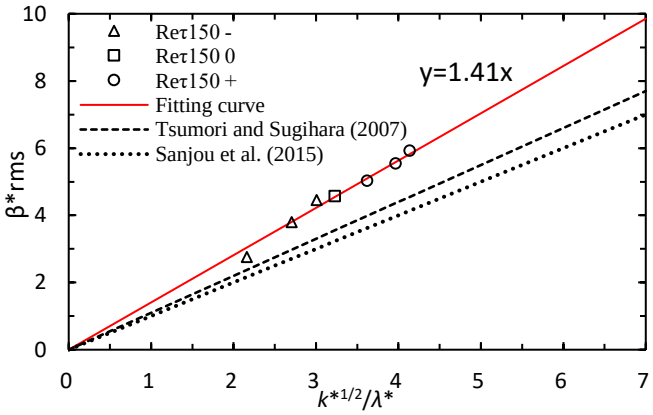

Figure 3. Scaling relation for surface divergence based on Taylor micro scale (DNS, $Re_\tau = 150$)

Figure 1 shows the response of the averaged streamwise velocity distributions to τ_s^* obtained from DNS under the condition of $Re_\tau = 150$. This figure demonstrates that the positive or negative vertical shear of the velocity is formed near the water surface according to the sign and magnitude of the surface shear stress. In addition, in the case of the positive surface shear stress, it can be seen that the inflection point appears in the velocity distribution. The most interesting point is that when a negative shear stress is applied, the streamwise velocity around the half-water depth is obviously increased compared to that in the case of no shear stress. However, this tendency cannot be reproduced by the standard k-ε model for turbulence at high Reynolds numbers. The feature has been also confirmed from experimental results provided by Nezu et al. (2005). The physical mechanism has not been elucidated yet though this phenomenon is of very interest from a viewpoint of hydrodynamics. The response in the results from the k-ε model becomes smaller than that from DNS near the water surface, even though the surface shear stress takes the same value. This suggests that there is an unexplained mechanism to be considered in the vicinity of the water surface. Figure 2 shows the vertical distributions of the Reynolds stress obtained from the numerical results using by DNS. It is clear that they change linearly except for the regions near the bottom and the water surface according to the sign and magnitude of the surface shear stress.

The divergence of the horizontal velocities on the water surface, i.e., the surface divergence, is considered to be a significant parameter for scalar transport at the water surface. The surface divergence β^* is defined by

$$\beta^*(x^*, z^*, t) = \left(\frac{\partial u^*}{\partial x^*} + \frac{\partial w^*}{\partial z^*}\right)\Big|_{surface}, \tag{11}$$

where $u^*$and w^*represent the velocities in the $x^*$and z^*directions, respectively.

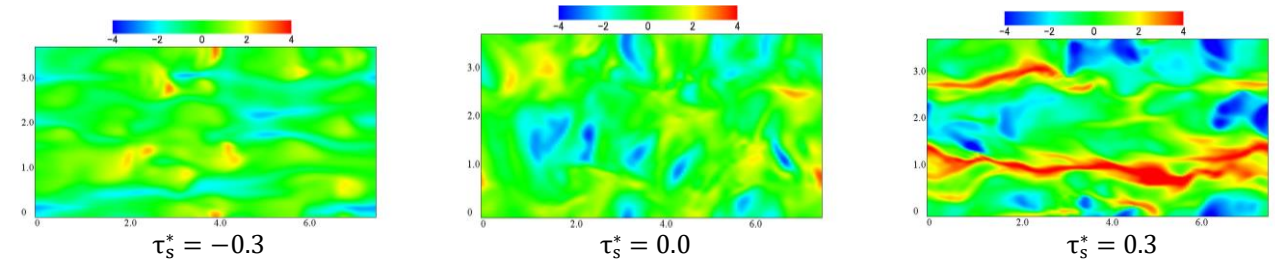

$\tau_s^* = -0.3$ $\tau_s^* = 0.0$ $\tau_s^* = 0.3$

(a) Streamwise velocity fluctuation on water surface

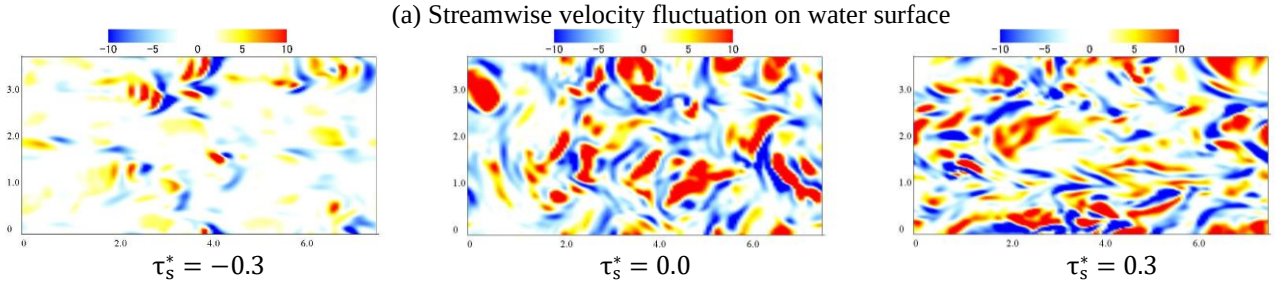

$\tau_s^* = -0.3$ $\tau_s^* = 0.0$ $\tau_s^* = 0.3$

(b) Surface divergence

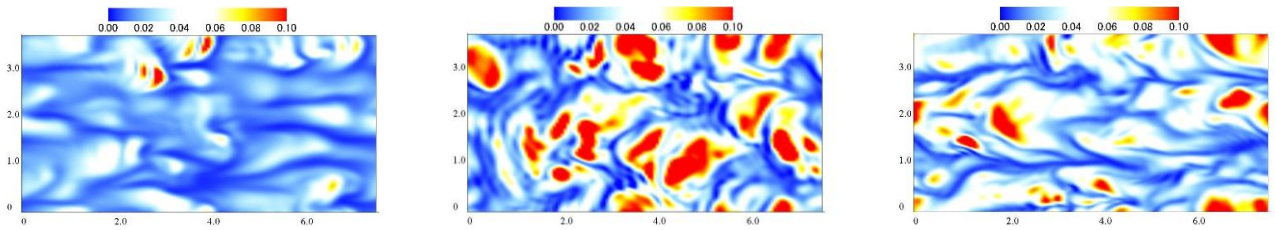

$\tau_s^* = -0.3$ $\tau_s^* = 0.0$ $\tau_s^* = 0.3$

(c) Scalar flux on water surface

Figure 4. Distributions of streamwise velocity fluctuation, surface divergence and scalar flux (DNS, $Re_\tau = 150$)

Figure 3 shows a scaling relation for the rms value of the surface divergence, expressed by using the Taylor microscale $\lambda^*$and the turbulent kinetic energy k^*. Also, λ^* has been calculated from the root mean squares of the velocity fluctuation and its spatial gradient. It is seen from the figure that this relation holds universally regardless of the sign and magnitude of the surface shear stress. This means that the surface divergence can be universally expressed on the Taylor microscale regardless of the action of shear stress on the water surface, but the proportionality constant is different from the experimental results of Sanjou et al. (2015), and Tsumori and Sugihara (2007). A further study is needed to explain quantitatively the reason for this difference.

Let us consider the case where the transport of a passive scalar such as dissolved gas drives from the gas phase to the water phase across the water surface. The scalar transport is induced by turbulent motions and the difference between the concentration at the surface C_s^* and that in the bulk C_b^*. In statistically-steady state, the scalar flux at the water surface F^*can be expressed by the following equation:

$$F^* = \frac{1}{Re_\tau Sc}\frac{\partial C^*}{\partial y^*}\bigg|_{surface} = k_L^*(C_s^* - C_b^*)\,. \tag{12}$$

Here the flux is defined to be positive downward from the water surface, k_L^* the gas transfer velocity, and *Sc* the Schmidt number. When the fluctuation of the water surface can be ignored and the concentration boundary layer of scalar becomes sufficiently thin compared to the scale of near-surface turbulent vortices because of high Schmidt number, the following analytical solution can be obtained from the advection-diffusion equation under the stagnation approximation (e.g., see Awaya and Abe,1971):

$$k_L^+ = \sqrt{\frac{2}{\pi}} Sc^{-\frac{1}{2}} \sqrt{\beta^+}\,, \tag{13}$$

where + indicates the dimensionless quantity in the form of the viscous wall unit. It is possible to discuss the effects of the surface shear stress through the comparison of the numerical results with Eq. (13).

In order to investigate quantitatively physical parameters that control the surface scalar transport, we define the cross-correlation coefficients between the surface scalar flux and turbulent characteristic quantities as follows:

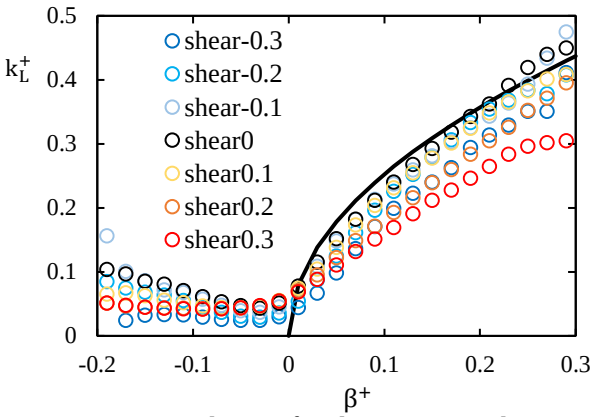

Figure 5. Relation of scalar transport velocity with surface divergence: Analytical solution and DNS ($Re_\tau = 150$)

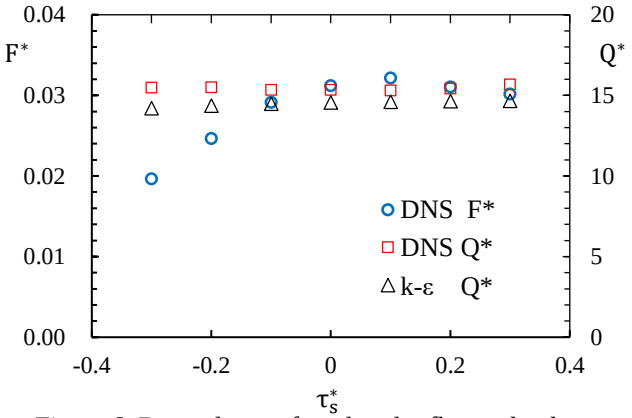

Figure 6. Dependence of total scalar flux and volume flow rate on surface shear stress: DNS ($Re_\tau = 150$) and k-ε model

$$\left.\begin{aligned} C_x(r_x) &= \frac{\langle F^{*\prime}(x^*,z^*)A^{*\prime}(x^*+r_x,z^*)\rangle}{F^*_{rms}A^*_{rms}} \quad (x^*\text{: steamwise direction}) \\ C_z(r_z) &= \frac{\langle F^{*\prime}(x^*,z^*)A^{*\prime}(x^*,z^*+r_z)\rangle}{F^*_{rms}A^*_{rms}} \quad (z^*\text{: spanwise direction})\ . \end{aligned}\right\} \tag{14}$$

Here, r_x and r_z denote the distances in each direction from (x^*, z^*), respectively. Also, $F^{*\prime}(x^*, z^*)$ and $A^{*\prime}(x^*, z^*)$ are the fluctuation components of the surface flux and turbulent quantities at (x^*, z^*), indicating $F^{*\prime}(x^*, z^*) = F^*(x^*, z^*) - \langle F^*(x^*, z^*)\rangle$ and $A^{*\prime}(x^*, z^*) = A^*(x^*, z^*) - \langle A^*(x^*, z^*)\rangle$.

In this study, we consider the fluctuations of the surface divergence β^*, the vorticity ω_x^* in the streamwise direction, and the vorticity ω_z^* in the spanwise direction as the physical quantities of $A^{*\prime}$. That is, the cross-correlation coefficients express the degree of correlation between the scalar flux F and the respective physical quantities at the distances separated by r_x and r_z.

Figures 4(a) to (c) show the two-dimensionally projected snapshots of the streamwise velocity fluctuation, the surface divergence, and the surface scalar flux on the water surface, obtained by the numerical results from DNS in the cases of $Re_\tau = 150$ and $\tau_s^* = -0.3,\ 0.0,\ 0.3$, and the abscissa and the ordinate stand for the x^*direction and the z^*direction, respectively. In the case of $\tau_s^* = 0$, the negative velocity fluctuation region exists in a patch shape, and the positive surface divergence region is formed so as to correspond to them. The surface flux also increases intensively in those regions. For the respective velocity fluctuations of $\tau_s^* = -0.3$ and 0.3, the low-speed region and the high-speed one appear as streaky patterns, which are similar to the low-speed streaks observed close to the bottom surface. In addition, there are the patch areas deformed by the velocity shear, which correspond to the place at which the low-concentration fluid in the bulk region rises to the water surface. However, for the surface divergence and the scalar flux, there exists a great difference between the cases of $\tau_s^* = -0.3$ and 0.3. In the case of $\tau_s^* = -0.3$, the surface divergence and the scalar flux become considerably smaller than those of $\tau_s^* = 0$ and 0.3. Also, the degree of the agreement between the spatial patterns of the surface divergence and the scalar flux decreases in the case of $\tau_s^* = 0.3$, suggesting that the mechanism of scalar transport is governed by a certain dynamics other than the surface divergence.

Figure 5 shows comparisons between the local scalar transfer velocity and the numerical results from DNS. The solid line drawn in the figure shows the analytical solution of Eq. (13) and the numerical results have been filtered by the moving average in an infinitesimal interval of $\Delta\beta^* = 0.02$. When the surface shear stress is $\tau_s^* = 0$, the numerical result in the positive region of β^+ agrees well with the analytical solution, inapplicable to the negative region because of its definition. The scalar transfer velocities vary with the surface shear stress, and those when $\tau_s^* = 0.3$ and -0.3 become smaller compared to the case of $\tau_s^* = 0$. It is concluded from this figure that the scalar transfer velocity depends on the sign and magnitude of τ_s^*. In particular, the mechanism of scalar transport under large positive surface stress seems to change from the surface divergence to the other physical mechanism.

Figure 6 shows the dependence of the averaged scalar flux computed by DNS on the surface shear stress, and the shear-dependence of the volume flow rate obtained from both of DNS and the standard k-ε model. The volume flow rate almost conserves regardless of the surface shear stress for the both results simulated by DNS and k-ε model. This figure demonstrates that the scalar flux is obviously decreased in the region of $\tau_s^* < 0$,

whereas in the range of $\tau_s^* > 0$, the flux is almost kept to be constant. Such an asymmetry is consistent with the results shown in Fig. 4.

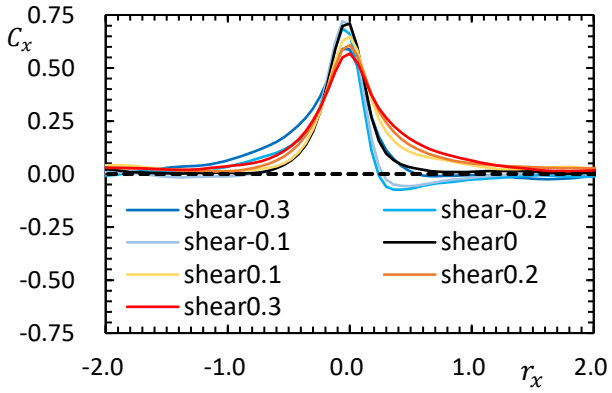

(a) Surface divergence β*

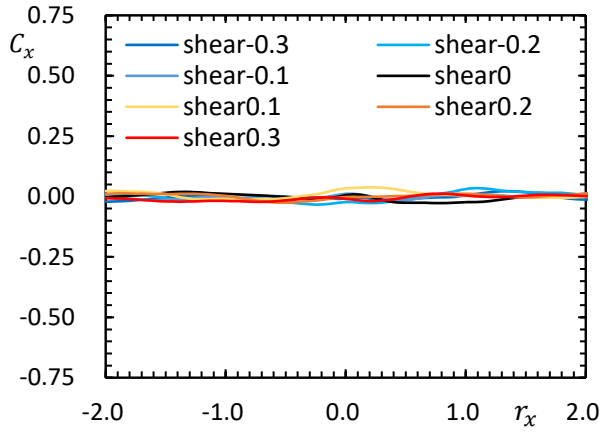

(b) Streamwise vorticity ω_x^*

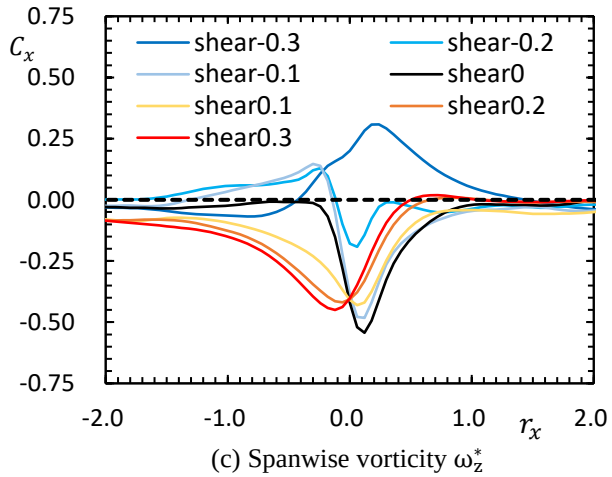

(c) Spanwise vorticity ω_z^*

Figure 7. Cross correlation for streamwise direction $C_x(r_x)$ (DNS, $Re_\tau = 150$)

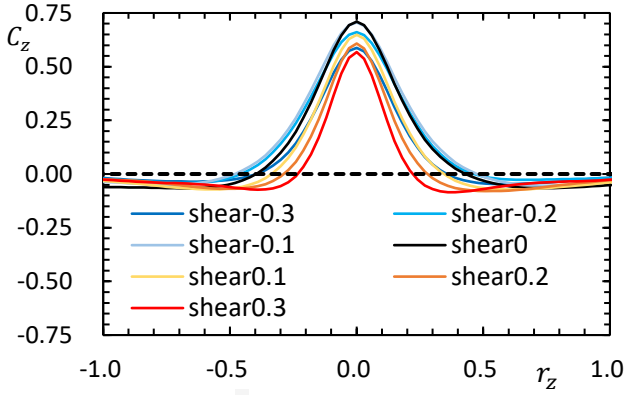

(a) Surface divergence β*

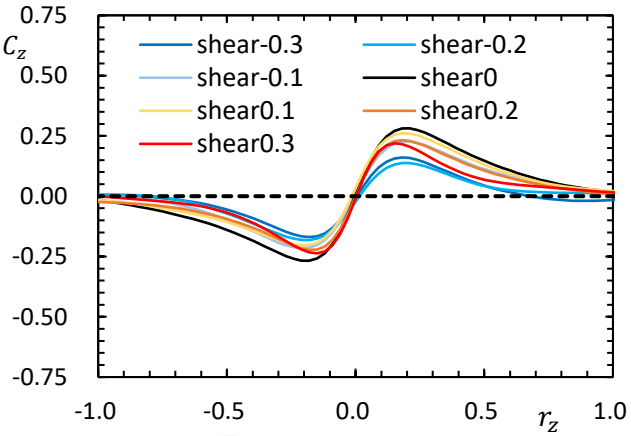

(b) Streamwise vorticity ω_x^*

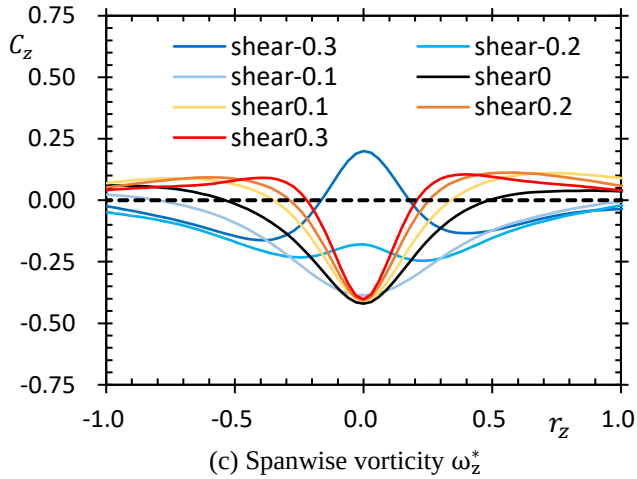

(c) Spanwise vorticity ω_z^*

Figure 8. Cross correlation for spanwise direction $C_z(r_z)$ (DNS, $Re_\tau = 150$)

Figures 7 and 8 show the cross-correlation coefficients among the scalar flux, the surface divergence and the vorticities in the streamwise and spanwise directions, where the vorticities have been calculated at the dimensionless depth of $y^* \approx 0.996$. First, let us discuss the correlations between the surface scalar flux and the surface divergence. The cross-correlation coefficient $C_x(r_x)$ when $\tau_s^* = 0$ for the relation with the surface divergence shown in Fig. 7 (a) is found to be symmetric with respect to the origin of $r_x = 0$, whereas for the other values of τ_s^*, it becomes asymmetric. When the positive shear stress, $C_x(r_x)$ increases relatively in the region of $r_x > 0$. Conversely, in the cases of $\tau_s^* = -0.1$ and -0.2, the downward overshoot of $C_x(r_x)$ is observed in the region of $r_x > 0$. In Figure 8(a), the cross-correlation coefficients $C_z(r_z)$ shows symmetric shapes with respect to $r_z = 0$ regardless of the sign and magnitude of τ_s^*. The maximum values of the cross-

correlation coefficients $C_x(r_x)$ and $C_z(r_z)$ take 0.75 approximately when $\tau_s^* = 0$, supporting that the surface divergence is an important physical quantity for describing the scalar flux at the water surface.

For the streamwise correlation of the flux with ω_x^* shown in Fig. 7(b), there is no correlation for the respective values of τ_s^*. This means that it is meaningless for the scalar transport to move the streamwise vortex line on target point in the streamwise direction. The values of $C_z(r_z)$ for ω_x^* in Fig. 8(b) is seen to be obviously antisymmetric with respect to $r_z = 0$. These facts indicate that the surface scalar flux increases when the vortex structure is arranged so as to induce an upward flow efficiently and make the concentration boundary layer of scalar much thinner. From the streamwise correlation with ω_z^* shown in Fig. 7(c), it is seen that the relation of $C_x(r_x)$ with τ_s^* becomes complicated especially in the case of the negative shear stress. Also, the correlation drawn in Fig. 8(c) shows symmetrical variation with respect to $r_z = 0$, but the behavior is complicated in the case of negative shear stress like that in Fig. 7(c). The characteristics of these correlations may be because the interaction of the shear flow turbulence with turbulence originated by the bursting near the bottom surface, and it is expected that understanding of the interaction contributes to the modeling of the air-water scalar transport.

4. CONCLUSIONS

We have investigated the response of open-channel turbulence to wind-driven surface shear stress by using the numerical methods of DNS and the standard k-ε model. It has been seen that the vertical distributions of the streamwise velocity and the Reynolds stress vary depending on the positive or negative sign of the surface shear stress. The numerical results from DNS have provided that under the condition of negative shear stress, the streamwise velocity around the half-water depth is increased than that in the case of no shear stress. The surface divergence calculated from DNS has been confirmed to be universally scaled with the Taylor microscale regardless of the positive or negative sign of the shear stress. Though the volume flow rate doesn't change regardless of the variation of the surface shear stress, the scalar flux at the water surface is found to be changed by the sign of the surface shear stress. In addition, the cross-correlation coefficients between the scalar flux and the physical quantities such as the surface divergence and the vorticities close to the water surface have been investigated to examine turbulent motions controlling the scalar transport at the water surface. It has been concluded from the cross-correlation coefficients that the scalar flux considerably increases when vortex structure is arranged so as to induce a strong upward flow toward the water surface.

ACKNOWLEDGMENTS

This work was partially supported by a Grant-in-Aid for Scientific Research (B) (Coordinator: Y. Sugihara, JSPS KAKENHI Grant Number JP19H02249) .

REFERENCES

Awaya, Y. and Abe, T. (1971). On turbulent characteristics and aeration rate at the water surface (II), *The 26th Annual Japan Society of Civil Engineers Congress* II, 491-492. (In Japanese)

Matsunaga, N. and Uzaki, K. (2002). Experimental Study on Secondary Circulations in Wind-Driven Currents, *Journal of Japan Society of Civil Engineers*, No.705 / II-59, pp.67-82. (In Japanese)

Nakayama, A. and Yokojima, S. (1999). Evaluation of Low-Reynolds-Number Turbulence Models as Applied to the Prediction of Open Channel Flows, *Journal of Japan Society of Civil Engineers*, No.628 / II-48, pp.131-148. (In Japanese)

Nezu, I., Fukutani, A., Yoshida, K. and Tarui, K. (2005). Experimental Study on Turbulence Characteristics and Gas Transfer in Adverse Wind-Driven Open-Channel Flows, *Journal of Applied Mechanics*, Vol.8, pp.911-918. (In Japanese)

Nezu, I., Yoshida, K. and Tarui, K. (2004). Study on Relationship between Turbulence Structures and Water Surface Fluctuations in Wind-Driven Open-Channel Flows, *Annual Journal of Hydraulic Engineering*, Vol. 48, pp.517-522 (In Japanese)

Sanjou, M. and Nezu, I. (2011). Turbulence Structure and Coherent Vortices in Open-Channel Flows with Wind-Induced Water Waves, *Environmental Fluid Mechanics*, Vol.11, pp.113-131.

Sanjou, M., Takahashi, K., Toda, K. (2015). Hydrodynamic Effects of Strip Roughness on Surface Velocity Divergence in Open-Channel Turbulent Flows, *Journal of Japan Society of Civil Engineers*, Ser. B1 (Hydraulic Engineering) Vol.71, No.1, pp.1-10. (In Japanese)

Sugihara, Y., Nakagawa, D. and Shiono, K. (2011). Direct Numerical Simulation of gas transfer at the air-water interface, *Journal of Japan Society of Civil Engineers*, Ser. B2 (Coastal Engineering), Vol.67, No.2, pp.71-75. (In Japanese)

Tominaga, A. (2010). Turbulence Dynamics in River Flows and Its Modeling, Special Issue: Water Engineering for Disaster Prevention, *Nagare*, Vol.29, pp.167-176. (In Japanese)

Tsumori, H. and Sugihara, Y. (2007). Lengthscales of motion that control the air-water gas transfer in grid-stirred turbulence, *J. Marine Systems*, Vol. 66, pp.6-18.